DOI: 10.54254/2753-8818/2026.HZ30765

Morphology Matters: The Dominant Impact of Ice Geometry on Airfoil Performance Decay

David Wu

Manhasset High School, Manhasset, USA
sanshengwu.david@gmail.com

Abstract. Aircraft icing is one of the most significant hazards affecting aviation safety, often leading to degraded aerodynamic performance, thus causing accidents. Research needs to be conducted in order to fully investigate the specific aerodynamic effect of different types and sizes of icing conditions. In this study, the aerodynamic characteristics of iced airfoils were investigated using computational fluid dynamics (CFD) simulations, with emphasis on their impact on lift, drag, and stall characteristics. Three typical ice morphologies, which were the horn ice, rime ice and glaze ice, were considered, and their influence on overall aerodynamic efficiency was analyzed with both numerical lifting data and airflow contour figures. Each icing conditions were also sub-divided into 4 different sizing (0.75x, 1x, 1.25x, 1.5x) to be investigated for the effect of different sized icings profiles. For the methodology, CFD simulations were developed, with organized domain and boundary condition setup and meshing. Results demonstrated that the glaze ice has the most detrimental influence on lift performance, only providing 16.5% of the original lift-to-drag ratio, and rime ice has the most moderate reduction, while still only having 38.4% of the initial one. Moreover, ice size and shape variations of horn and glaze ice revealed strong negative relationship between ice size and aerodynamic performance, while rime ice did not show evident correlations. These data would lead to a conclusion that icing conditions in general are harmful to the aerodynamic performance, and sizing variances of icing profile reveal complicated airflow characteristic changes.

Keywords: Icing airfoil, CFD, aerodynamics

1. Introduction

Aviation safety is the absolute top consideration during the invention, evaluation and upgrade of aircraft. The aircraft should be well designed to operate safely in all suitable and probable flight environments. Admittedly, in some weather conditions, the aircraft will exhibit a certain level of danger, including wind shears, thunderstorms, and cold conditions, where icing would occur on the aircraft. The top goal of aircraft producers and operators would then be to minimize the risk posed by those dangerous situations and ensure the safe operation of the aircraft.

Specifically for aircraft icing, it represents one of the most critical safety challenges in aviation, particularly under sub-freezing conditions, where ice accretion on aerodynamic surfaces can lead to severe performance degradation. The formation of ice alters the intended airfoil geometry, disrupting

DOI: 10.54254/2753-8818/2026.HZ30765

smooth airflow and inducing premature flow separation, which consequently diminishes lift generation while substantially increasing drag and stall susceptibility [1]. In the flight safety alerts of National Transportation Safety Board (NTSB) [2], icing was one of the major topics to be discussed and warned, showing it as a severe threat to the safety of the aircraft.These aerodynamic penalties have been directly implicated in numerous aviation accidents throughout history, underscoring the imperative for continued research in this field.

An example of large aircraft crashes due to icing would be the China Eastern Air Flight 5210 in 2004. The airplane did not receive deicing before takeoff [3], causing the airfoil to not produce an adequate amount of lift for the aircraft to continue rising, eventually causing a total of 55 fatalities. Another example would be US Airways flight 405 in 1992. The airplane also faced icing on its airfoils during takeoff [4], leading to the final crash and caused 27 fatalities with multiple injuries [5]. Other than these big and famous accidents, the major problem of icing occurred especially on those small General Aviation Aircraft (GA), where those types lack complete examinations or design redundancies to survive from icing. In cold seasons of every year there have been reports regarding the crashes or emergencies of those aircraft due to icing. From all those incidents it would be seen that icing would be treated as a serious hazard for flight safety and related research is worth conducting to investigate the detailed effect of icing on the aerodynamic performance of the aircraft.

To specify the effect of icing to the aerodynamic performance of the aircraft, the majority of past researches and administrations [6-8] distinguished icing profiles on airfoils to 3 main types. The first one is rime ice. It is a smaller sized icing formation that occurs when small water droplets hit the airfoil surface and forms a rough ice that would conform to the original shape of the airfoil. Next one is glaze ice. Formed by larger and colder water droplets, glaze ice would have a thicker icing layer and would grow forward irregularly from the airfoil surface, significantly altering the initial dimension of the airfoil. There is a subtype to the glaze ice, called horn ice, that would have the most dramatic change to the dimensions. In this type of icing the ice would extend so far forward that it would form 2 “horns” in front, causing dramatic alterations in airflow conditions. The last large type is the mixed ice, which is simply the combination of both the glaze and the rime ice and would occur in conditions with varied sized droplets and temperatures. Most of the icing related researches had utilized this classification and conducted related studies accordingly.

Previous research efforts have primarily investigated icing effects through experimental testing and computational simulations. Nath et al. [9] examining horn, rime, and glaze ice formations on NACA 0012 airfoils demonstrated substantial lift reduction and drag increases, with horn ice proving particularly detrimental due to its pronounced geometric disruption. These studies also revealed complex interactions between surface roughness characteristics and aerodynamic response. However, a significant limitation of existing research lies in the frequent use of idealized ice geometries that fail to accurately represent realistic accretion patterns formed under actual flight conditions. This simplification reduces the practical applicability of resulting performance predictions and may overlook critical flow phenomena associated with more complex ice formations. This limitation of ignoring actual icing conditions was also frequently seen in numerous other previous researches.

This present study addresses these limitations through a systematic investigation of aerodynamic performance degradation caused by various ice morphologies and geometric parameters, originating from the icing simulation of National Aeronautics and Space Administration (NASA). This research employs high-fidelity computational fluid dynamics to examine how specific ice geometry characteristics—including type, size, and shape variations—influence separation behavior and overall aerodynamic efficiency. The investigation focuses specifically on 2 primary objectives:

DOI: 10.54254/2753-8818/2026.HZ30765

quantifying the aerodynamic penalties associated with different icing morphologies (horn, rime, and glaze ice) and analyzing the sensitivity of performance degradation to precise geometric dimensions of ice formations. The data acquired in this study would then be valuable to the future construction of icing dimension models and optimization of the airfoils.

The Computational Fluid Dynamics System (CFD system) was used to proceed with those required simulations of airfoil models in order for the researchers to acquire reliable data. CFDs would be an effective model for simulating these aircraft-related situations and any other aeronautical engineering problems, as the instrument was able to replicate the actual or similar conditions of an aircraft during flight [10]. The CFDs are also capable of simulating the activity of airflow around an aircraft during a flight and would be able to accurately predict both the lift and drag which had been recorded in the software. In this study, the CFD would be used to simulate several different iced airfoils, deciphering the performance of each iced conditions. Out of all the CFD systems, ANSYS Fluent would be the absolute top simulation tool, as proved by the fact that the majority of the researchers conducting aerodynamics related studies used Fluent. Therefore, ANSYS Fluent will be the CFD system in this study.

Based on all those information above, the need and purpose of this current study would be clearly seen, which would be to investigate the detailed aerodynamic performance of the airfoil when encountering realistic icing conditions, thus providing valuable data to assist both the aircraft producers and operators, determining the specific effect and possible solutions of different icing conditions. To achieve this, 3 main types of icing conditions, being the glaze ice, horn ice and rime ice, would be considered; Different sizings of each specific type would be modeled; Multiple data exhibition pathways, including lift and drag coefficient, pressure coefficient and vorticity magnitude, would be utilized. Based on all the previous knowledge, hypotheses were also formed that icing conditions would have a negative effect on the airfoil by distorting airflow and the horn ice would have the worst performance out of all types tested, since its spiked horns would provide largest dimension alteration to the aircraft.

This paper would be structured to provide comprehensive documentation of the methodology and findings. The methodology section details the numerical framework, including governing equations, computational domain design, boundary conditions, and meshing configurations. Sections 3 and 4 present thorough analysis of aerodynamic performance under various icing conditions, with particular emphasis on the relationship between ice geometry type and size and resulting flow separation characteristics. Finally, summary section provides concluding remarks and discusses promising directions for future research on aircraft icing aerodynamics.

2. Numerical methodology

2.1. Governing equations and turbulence modeling

The aerodynamic characteristics of iced airfoils were investigated using steady-state Reynolds-Averaged Navier-Stokes (RANS) simulations. This governing equation accounts for incompressible flow and consist of the continuity and momentum conservation equations:

$$\nabla \cdot \mathbf{u} = 0 \tag{1}$$

$$\frac{\partial \mathbf{u}}{\partial t} + \nabla \cdot (\mathbf{u} \otimes \mathbf{u}) = -\frac{1}{\rho} \nabla p + \nu \nabla^2 \mathbf{u} + \nabla \cdot \tau_R \tag{2}$$

DOI: 10.54254/2753-8818/2026.HZ30765

In the equation, $\mathbf{u}$ represents the velocity vector; p denotes the pressure; ρ is the fluid density; ν is the kinematic viscosity; τ_R is the Reynolds stress tensor requiring turbulence modeling closure.

For turbulence closure, the standard k - ε model was employed, which solves two additional transport equations for turbulent kinetic energy (k) and its dissipation rate (ε):

$$\frac{\partial k}{\partial t} + \nabla \cdot (k\mathbf{u}) = \nabla \cdot \left[\left(\nu + \frac{\nu_t}{\sigma_k}\right)\nabla k\right] + P_k - \varepsilon \tag{3}$$

$$\frac{\partial \varepsilon}{\partial t} + \nabla \cdot (\varepsilon\mathbf{u}) = \nabla \cdot \left[\left(\nu + \frac{\nu_t}{\sigma_\varepsilon}\right)\nabla \varepsilon\right] + C_{1\varepsilon}\frac{\varepsilon}{k}P_k - C_{2\varepsilon}\frac{\varepsilon^2}{k} \tag{4}$$

where $\nu_t = C_\mu k^2/\varepsilon$ represents the turbulent viscosity, P_k is the production term of turbulent kinetic energy, and the model constants are assigned standard values: $C_{1\varepsilon} = 1.44$, $C_{2\varepsilon} = 1.92$, $C_\mu = 0.09$, $\sigma_k = 1.0$, and $\sigma_\varepsilon = 1.3$.

2.2. Geometric modeling of iced airfoils

The icing geometries used in this study were based on experimental data from icing simulations conducted by NASA [11]. In NASA's research, airfoils were subjected to various environmental conditions, including different temperatures, angles of attack (AOAs), and airspeeds, to encompass all possible flight scenarios. Multiple iced airfoil profiles were generated, each exhibiting distinct icing sizes and types. Given NASA's status as the leading authority in aeronautics, the results of these simulations were considered sufficiently reliable to serve as the foundation for the geometries in this study.

Of the several major icing types investigated by NASA, three were selected for evaluation: horn ice, glaze ice, and rime ice. Mixed ice, being a more complex combination of the aforementioned types, was excluded from this study due to its intricate characteristics and the difficulty in defining consistent dimensional alterations. Geometries corresponding to NASA simulations, specifically being Runs ED0712, ED0714, and ED0724, were chosen as the representative icing profiles for horn ice, glaze ice, and rime ice, respectively.

The icing geometries from these simulations were then acquired and served as the "normal icing geometry" (1x size) for the computational fluid dynamics (CFD) simulations conducted in this research. For each icing type, three additional scaled geometries were constructed: 1.25x, 1.5x, and 0.75x, achieved by modifying the size or length of the ice on the airfoil. In total, 12 groups of icing conditions were tested, with the control group (airfoil without ice) bringing the total to 13 experimental configurations. In NASA's experiments, the base airfoil used for all three icing conditions was the NACA 23012 airfoil, a widely used airfoil for multiple generations of general aviation aircraft [12]. This aircraft type, as mentioned earlier, is particularly vulnerable to icing, making its use in simulations highly relevant for the study. Consequently, the NACA 23012 airfoil was applied to all 13 models in the current study.

For the 3D modeling of the airfoils, the geometries were scaled down to a final chord length of 1300 millimeters (mm) for the NACA 23012 airfoil. As the NASA datasets only provided the front portion of the iced geometries, the full 2D airfoil data was obtained from Airfoil Tools, a widely recognized database of common airfoils, and integrated with the icing geometries to both complete the airfoil shape and verify the accuracy of the initial front dimensions. This process was repeated for all 12 experimental groups.

DOI: 10.54254/2753-8818/2026.HZ30765

2.3. Computational domain and boundary conditions

The computational domain would then be constructed for each airfoil constructed. This domain would be able to define a region of calculation and evaluation for the software and the computers in the later simulations. The domain should be large enough (at least 8 times the chord length in length and 4 height) to ensure the validity and accuracy of the airflow and simulational calculations. The inlet part of the domain should also be circular to handle the possible AOA difference in the simulation, where for the CFD systems the AOA were usually achieved by changing the x and y component airflow amount, and a circular inlet could better deal with this alteration. Specifying these rules, the flow domains for all the airfoils in this research were set to be a rectangle with a semicircle connected to its front edge, and the airfoil located in the center. The rectangle has a length of 12000mm and a width of 8000 mm, thus setting the radius of the semicircle as 4000mm. These would then roughly convert to a length of 12 chord length and width of 6 chord length for the entire flow domain.

As mentioned, the velocity inlet was set to be the entire circular side of the semicircle, and the flow speed was set to be 50 m/s, converting to a Reynold number of 5.0×10^5 based on the chord length. It is also worth noting that a 5 degree AOA was modeled by an x flow component of 0.9962 and y flow component of 0.0872. A 4-6 degree of AOA was estimated to be the most optimistic and appropriate cruising AOA for the 23012 airfoil [13], legitimizing the setting for a 5 degree AOA. Additionally, the turbulence intensity was set to 1% with a turbulence viscosity ratio of 10. The pressure outlet was defined to be the far side of the rectangle, with the outlet boundary employing a pressure outlet condition with zero gauge pressure. Symmetry conditions were applied to the top and bottom boundaries, and the constructed airfoil geometry was treated as a no-slip wall with enhanced wall treatment, where all the data will be gathered from.

2.4. Meshing

Meshing is a process required for most of the CFD simulations. It would be able to break down curved and complicated geometries into simple triangles or quadrilaterals in order to make the geometries able to be calculated by the equations and computers. When constructing meshing conditions, it would be optimistic to minimize the meshing scale to show more detailed conditions of the geometry, while the scale should not be too small, where increased nodes will dramatically increase the calculation time for the geometry. Considering this comprehensively, the meshing scale was set to be 20mm for all the simulations in order to balance the need for both sides. This will eventually lead to a total node number of roughly 250000, with the difference in airfoil and icing geometries entailing slight variations. Considering the fact that the simulation was 2D only with only one single airfoil involved for each simulation, this number would be convincing enough.

DOI: 10.54254/2753-8818/2026.HZ30765

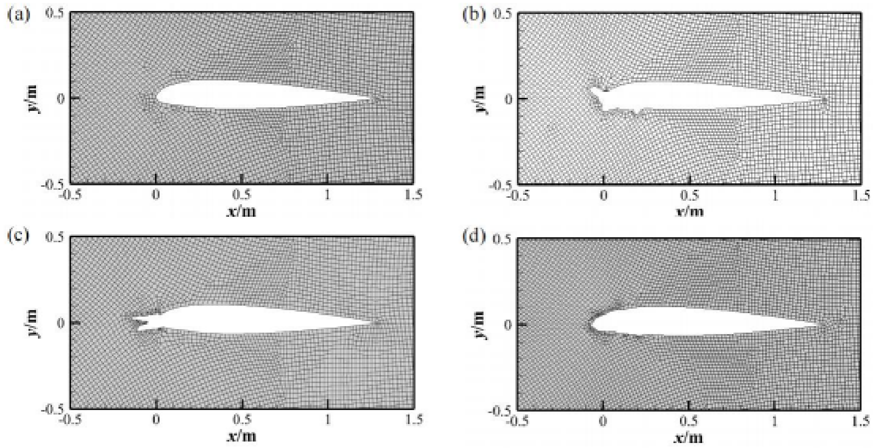

Figure 1. Mesh configurations for: (a) smooth airfoil, (b) iced airfoil with glaze ice, (c) iced airfoil with horn ice, and (d) iced airfoil with rime ice

Figure 1 presents the mesh configurations used for simulating airflow around different types of airfoils under icing conditions. Panel (a) shows the mesh for a smooth airfoil, serving as the baseline for comparison. Panels (b), (c), and (d) illustrate the meshes for iced airfoils, each with distinct types of ice: glaze ice, horn ice, and rime ice, respectively. All the meshes are refined near the airfoil surface.

2.5. Solution methodology and data collection

After establishing the mesh and all other presettings, simulations were conducted using a pressure-based coupled algorithm with second-order spatial discretization schemes in ANSYS Fluent. Various data were recorded and output to analyze the specific effects of the icing. To assess the impact on lifting performance, the lift coefficient (C_l) and drag coefficient (C_d) were directly recorded in Fluent. These coefficients allow for a more comprehensive comparison of lift and drag variations across different geometries with different dimensions, as opposed to simple lift forces in newtons. By factoring in airspeed, air density, and wing area, C_l and C_d provide a more thorough performance comparison between experimental and control groups.

The drag coefficient C_d is defined as:

$$C_d = \frac{F_d}{\frac{1}{2}\rho U^2 A} \tag{5}$$

where F_d is the drag force, ρ is the air density, U is the freestream velocity, and A is the reference area of the airfoil.

Similarly, the lift coefficient C_l is given by:

$$C_l = \frac{F_l}{\frac{1}{2}\rho U^2 A} \tag{6}$$

where F_l is the lift force. The ratio of the drag coefficient to the lift coefficient, known as the L/D ratio, provides a critical measure of the airfoil's overall performance. The L/D ratio is expressed as:

DOI: 10.54254/2753-8818/2026.HZ30765

$$\text{L/D Ratio} = \frac{C_l}{C_d} \tag{7}$$

This ratio is of paramount importance in evaluating aircraft lifting performance, as it reflects the airfoil's ability to generate lift while minimizing drag. It integrates the separate lift and drag measurements into a single performance indicator, which may otherwise appear disjointed when considered independently.

Despite the numerical lifting data, additional contour plots were constructed for each test case to provide a comprehensive understanding of the airflow conditions encountered by the iced airfoils. The first contour represents the pressure coefficient, which illustrates the pressure distribution around the airfoil. Since the pressure difference between the upper and lower surfaces of the airfoil is the primary source of lift, this contour helps validate the numerical lifting data by corroborating the pressure field's contribution to the lift generation.

The second contour presents the x-velocity magnitude (in m/s) along with airflow streamlines. According to Bernoulli's principle, the flow velocity directly influences the pressure distribution and, consequently, the lift around the airfoil. This contour serves as key evidence to explain the specific conditions of lift generation. Additionally, the streamlines provide insights into the directionality of the flow and highlight the formation of vortices.

The third contour shows the vorticity magnitude, which allows for the identification of vortices within the flow. These data are crucial for assessing the impact of icing on the flow structure, as the presence and intensity of vortices can significantly affect the aerodynamic performance of the airfoil.

Together, these contour plots provide essential insights into the flow characteristics and aerodynamic performance of the airfoils under varying icing conditions, offering a comprehensive picture of the effects of icing on the airflow and lift generation.

3. Effect of the ice type on the airfoil aerodynamics

3.1. Lift performance

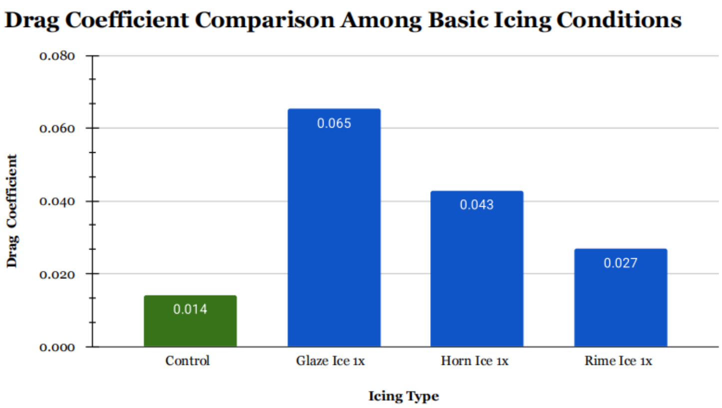

Figure 2. Comparison of drag coefficients for the smooth airfoil, iced airfoil with glaze ice, iced airfoil with horn ice, and iced airfoil with rime ice

DOI: 10.54254/2753-8818/2026.HZ30765

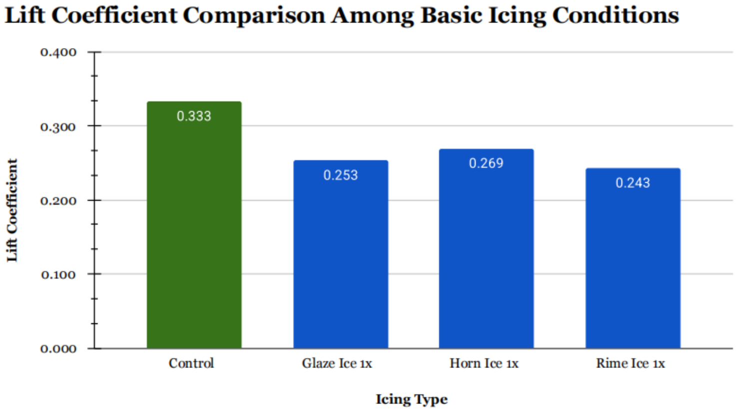

Figure 3. Comparison of lift coefficients for the smooth airfoil, iced airfoil with glaze ice, iced airfoil with horn ice, and iced airfoil with rime ice

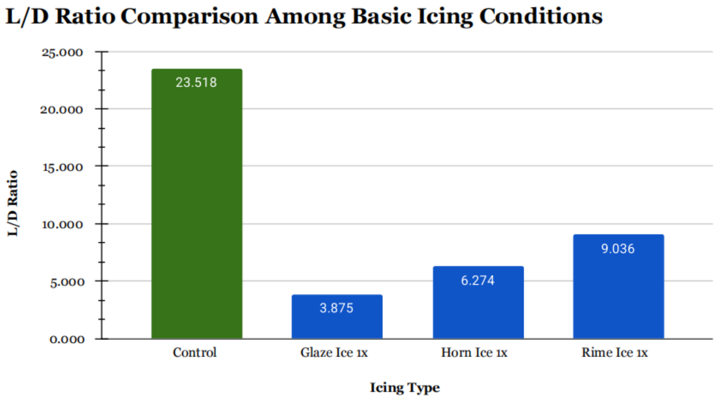

Figure 4. Comparison of L/D Ratio for the smooth airfoil, iced airfoil with glaze ice, iced airfoil with horn ice, and iced airfoil with rime ice

In the 3 figures above, the lift coefficient (Figure 2), drag coefficient (Figure 3) and L/D Ratio (Figure 4) for the glaze, horn and rime ice are compared with the clean airfoil. The x-axes of the bar graphs represent the airfoil type, and the y-axes represent lifting data, differing for each graph. Each data of the lift and drag coefficient was acquired from the last iteration output of the simulations, which guaranteed its accuracy; The numbers were rounded to the nearest thousandth to ensure the validity.

It was known that a high lift coefficient and L/D Ratio and a low drag coefficient would always indicate a better lifting performance. Then, looking at the trends of each graph, it was clearly seen that all 3 of the icing conditions showed much worse lifting performances compared to the smooth airfoil: The rime ice had an almost 90% increase in drag coefficient and a 27% decrease in lift coefficient, resulting in an deduction of L/D Ratio of 61%; The horn ice received a 203% increase in drag and a 19% increase in lift, causing it to have an L/D Ratio diminish of 73.3%; The worst being the glaze ice, having an increased drag of 240% and a decreased lift of 24%, directly lead to a total reduction of 83.5% in L/D Ratio. All of these would be seen as an extremely high constriction in lift generating efficiency of the airfoil, which may immediately lead to the occurrence of the stall situations. As a result, it would be confident to declare that the accumulation of ice on the airfoil

DOI: 10.54254/2753-8818/2026.HZ30765

would pose a significant risk to the flight stability and availability, which aligns with multiple other literature that all found the severe reduction of lifting data caused by icing.

Taking a more detailed analysis of the trends, it was found that the L/D Ratio reduction could be mainly ascribed to the severe decrease in drag coefficient, and the lift coefficient did not receive such a copious decrease. This means that the airfoil still maintained the ability to generate lift by the pressure difference between the top and bottom side after encountering icing conditions, while the accumulation of ice in the leading edge may cause the dramatic increase in skin friction drag and interference drag, which was reflected in the drag coefficient data. It was also found that all 3 types of icing had relatively similar lift coefficient reductions while totally different drag increase amounts. This could be caused by the specific dimensions of the ice in the leading edge that led to a distinction in the extra frictions faced, causing different drag data. These scenarios and potential explanations could be further clarified and exemplified by looking at the contour figures shown below.

3.2. Flow field analysis

The 3 contour figures shown here each represent the pressure coefficient (Cp)(Figure 6), velocity magnitude (with streamlines)(Figure 5), and vorticity magnitude (Figure 7) of the 3 icing conditions and the smooth airfoil. Each contour contains 4 sub contours, each representing one icing condition, as indicated in the captions of each figure. Each contour shares the same legend and key with the same colors representing the same value, as shown in the right side of the combination of the figures. As mentioned earlier, these figures would be able to provide a good visual for the airflow characteristics and supporting evidence for the trends observed in the lifting data performance section.

First, observing the x-component velocity contours, they basically show the airflow speed and directions. In the figures, the smooth airfoil showed streamlines with curves perfectly aligned with the shapes of the airfoil and also exhibited a decrease in airflow speed near airfoil surfaces, indicating a good control of the airflow. This means that the airflow will tally the design purpose of the airfoil perfectly, which is to create lift. No other locations had shown a severe moderation in airflow velocity, meaning that the airflow is stable and ideal to support lift creations. The 3 iced airfoils, however, showed totally different situations. The rime ice seemed to be the one having the most aligned airflow velocity to the control, while still have a slightly augmented zone of flow speed decrease in the leading edge, proposing a decrease in lifting performance; The horn ice figure yielded an even more erratic flow speed, with a severe airflow speed decrease in between its horns. This is understandable since the airflow was basically trapped in between the horns, shown by one particular flow streamline that was sucked into the horn and was not able to go around the airfoil. The glaze ice performed the worst, with plenty of flow speed reductions in behind the ice, where the entire airfoil surfaces seemed to be affected. Two vortices were immediately observed right behind icing profiles, further verifying the fact that the airflow was blocked by the ice to function onto the airfoil to provide lift.

DOI: 10.54254/2753-8818/2026.HZ30765

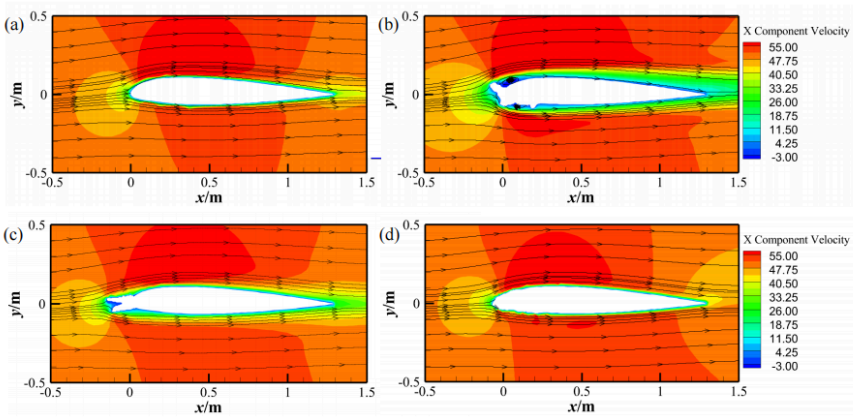

Figure 5. Contours of the $x-$ component velocity for: (a) smooth airfoil, (b) iced airfoil with glaze ice, (c) iced airfoil with horn ice, and (d) iced airfoil with rime ice

Second, the pressure coefficient graph showed the pressure conditions, the major factor determining the ability for the airfoil to provide lift, of the 4 airfoils. The control airfoil, again, showed an ideal pressure condition, with the pressure being smoothly higher at the upper surface of the airfoil. The rime ice showed almost the same pressure distribution, with only small changes observed at the icing profile part, which is caused by the irregular shape of the ice, leading to a relatively small degree of lift reduction. The glaze and horn ice, however, proposed severe changes to the pressure profile, which would definitely lead to a larger lifting performance decrease. Worthy to be notified, the horn ice airfoil showed a high pressure region in between the horns, aligning with the results of the velocity contour. All these changes in pressure could be succumbed to the dramatic airfoil appearance change brought by the icing conditions.

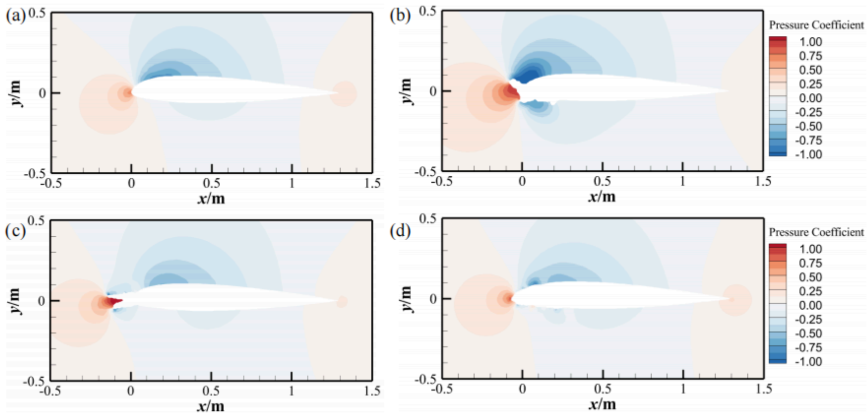

Figure 6. Contours of the pressure coefficient for: (a) smooth airfoil, (b) iced airfoil with glaze ice, (c) iced airfoil with horn ice, and (d) iced airfoil with rime ice

DOI: 10.54254/2753-8818/2026.HZ30765

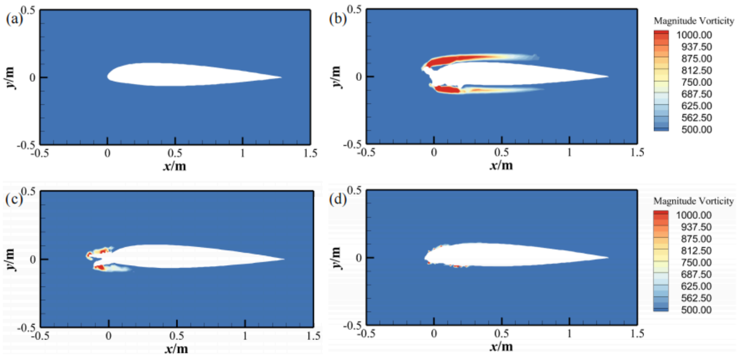

Figure 7. Contours of the pressure coefficient for: (a) smooth airfoil, (b) iced airfoil with glaze ice, (c) iced airfoil with horn ice, and (d) iced airfoil with rime ice

Last, the vorticity magnitude graph showed the potential occurrence of vortices of the airfoil. The majority of the times in flight the vortices are not wanted since it disturbs the original airflow structure. The smooth airfoil, which substantiates this unwillingness to vortices, did not show any evidence of a vortex. Due to the rough surface of the ice, the 3 experimental groups had all exhibited some degree of vortices. The rime ice and the horn ice all showed only a localized vortex appearance that did not affect the entire airfoil, which could potentially be explained by the small size of the defected profile (rime ice) or the far distance of the occurrence place (horn ice). The glaze ice, however, showed hazardous vortices at both the top and the bottom of the airfoil, which will impact the airflow conditions significantly. This is undoubtedly associated with the large size of the ice and the fact that it was right attached to the main airfoil.

To summarize these contour figures, they served as an optimistic evidence provider and perfectly supplemented each other to provide complementary visuals for analysis of the iced profiles. The reasoning for the dramatic increase of the drag coefficient is validated by these figures as the occurrence of vortices or chaotic airflow conditions that caused a dramatic increase in airflow frictions. Although not as severe as the drag increase, this would also interrupt the normal lift creating of the airfoil, as verified by the pressure coefficient graph that showed increased unwilling pressure conditions.

4. Effect of ice geometry size on airfoil aerodynamics

4.1. Aerodynamic performance

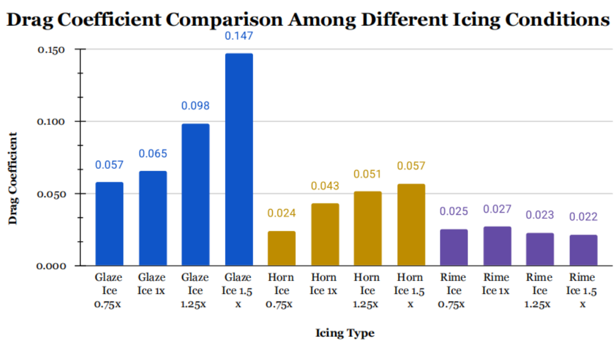

Figure 8. Comparison of drag coefficients for the ice airfoil with glaze ice, horn ice and rime ice, each having 4 sizes of 0.75x, 1x, 1.25x and 1.5x

DOI: 10.54254/2753-8818/2026.HZ30765

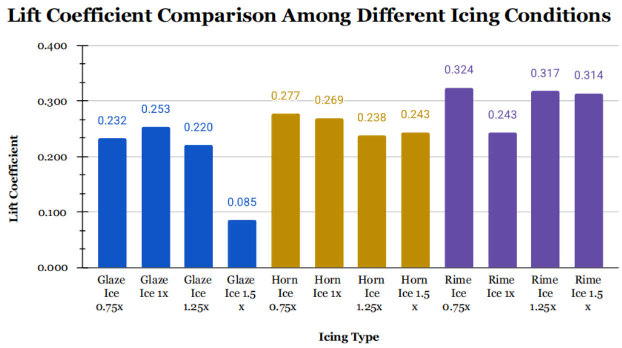

Figure 9. Comparison of lift coefficients for the ice airfoil with glaze ice, horn ice and rime ice, each having 4 sizes of 0.75x, 1x, 1.25x and 1.5x

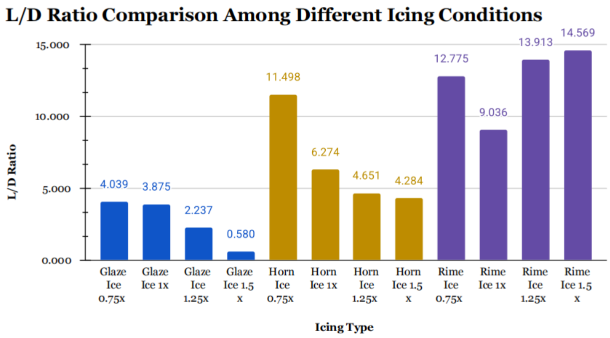

Figure 10. Comparison of L/D Ratio for the ice airfoil with glaze ice, horn ice and rime ice, each having 4 sizes of 0.75x, 1x, 1.25x and 1.5x

The 3 figures in this section still represent the lift coefficient, drag coefficient and L/D Ratio with the exact same y-axes arrangement. The x-axes, this time, represent 12 different icing conditions, with 4 sizes (0.75x, 1x, 1.25x and 1.5x icing size) from each major icing type of horn, glaze and rime ice. The blue colors represent the 4 types of glaze ice, the yellow being the 4 horn ice, and the purple as the 4 rime ice. As mentioned earlier in the methodology, the purpose of these figures are to compare the effect of icing specifically within each icing type.

Looking separately into the 3 distinct icing types, the first one in the discussion is the glaze ice. The lift coefficient was maintained fairly similar in the 0.75, 1 and 1.25x sizes, with an average around 0.235; The 1.5x sized ice airfoil, however, showed a dramatic drop in lift coefficient all the way down to 0.085, only 36% of the previous data. The only reason possible for causing this large drop would be ascribed to the total destruction of the boundary layer airflow caused by the enlarged icing profile that totally diminished the lift creating ability of the airfoil. This would be verified later by the contour figures. As seen in the drag coefficient graph, the glaze ice group also witnessed a dramatic drag coefficient increase for both the 1.25x and 1.5x glaze ice. These two combined then resulted in a profound L/D Ratio reduction for 1.25x and 1.5x glaze ice: The 1.25x glaze ice only outputted 57% of the L/D Ratio compared to the 1.0x glaze ice, and this number was further reduced to 25.9% for the 1.5x glaze ice. Such a dramatic decrease would guarantee a strong negative relationship between the size of the glaze ice and the lifting performance of the airfoil, especially considering that the 0.75x glaze ice saw a slight increase in L/D Ratio compared to the 1.0x.

Similar situations of negative relationship in L/D Ratio happened to the horn ice, where both the drag coefficient and the L/D Ratio followed the same trend despite observing a more improvement in data for the 0.75x horn ice compared to the relatively small degree of improvement by the 0.75x glaze ice. Such similarity could lead to the same reasonings for both the scenarios, which is likely the increased icing geometry that led to the increase in friction drag. Interestingly, the lift coefficient of the 4 horn ice did not see a clear enough decrease as the icing geometry amount increased, whereas those data showed no strong correlations with each other. The maximum difference of the lift coefficient was only 12%, occurring between the 0.75x and 1.5x horn ice, which, compared to the dramatic drag and L/D Ratio shift, seemed to be subtle. A possible explanation would be that the increase or decrease of the "horns" of the ice, which stretched horizontally outward only, did not affect the original airflow conditions of the airfoil as much compared to the glaze ice dimension changes.

The rime ice, compared to the clear change of the previous two types, showed almost no regular patterns in all 3 lifting data: The maximum and minimum drag coefficient occurred on 1x and 1.5x, respectively; The maximum and minimum lift coefficient appeared on 0.75x and 1x, with 1x having a dramatic decrease in data compared to the other 3; With this dramatic decrease the 1x ice took the lowest L/D Ratio, while the highest L/D Ratio is acquired by 1.5x. These irregular data patterns could lead to a conclusion that the thickness and length of the accumulated rime ice will not have a strong effect on the lift data of the aircraft, and the specific roughness or other dimensions could be the key of effect for rime ice. This could be explained by the fact that the rime ice has a more adjusted shape that basically replicated the dimensions of the airfoil, making the airfoil able to behave more stably compared to those angular and prominent glaze iced or horn iced airfoils.

4.2. Flow field analysis

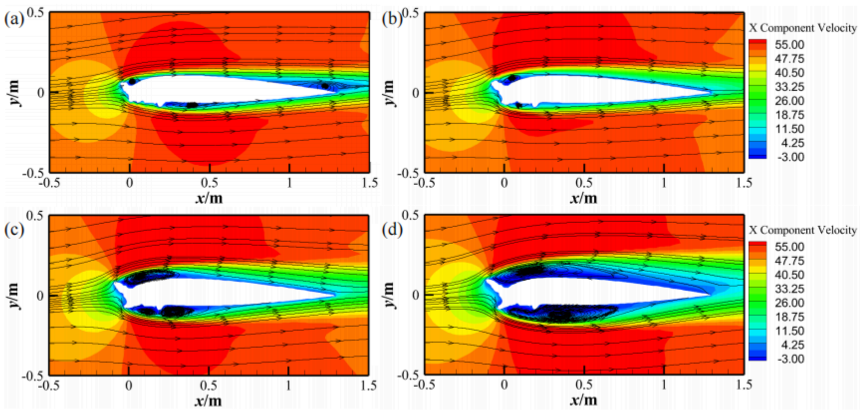

Figure 11. Contours of the $x-$ component velocity for: (a)0.75x glaze ice, (b)1x glaze ice, (c)1.25x glaze ice, and (d)1.5x glaze ice

DOI: 10.54254/2753-8818/2026.HZ30765

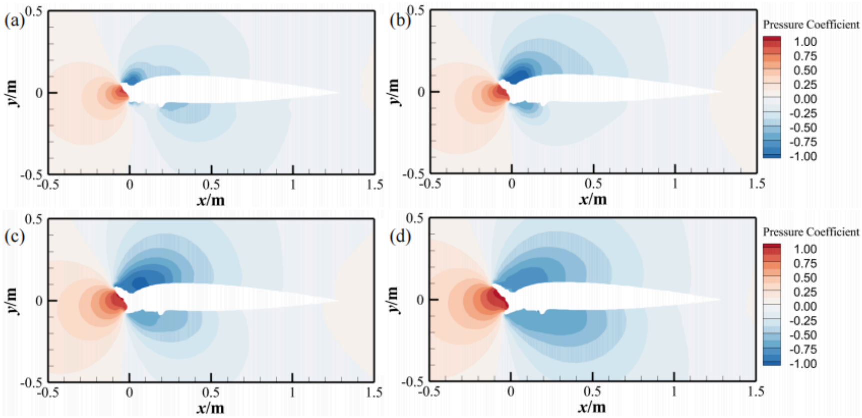

Figure 12. Contours of the pressure coefficient for: (a)0.75x glaze ice, (b)1x glaze ice, (c)1.25x glaze ice, and (d)1.5x glaze ice

First, figure 11, figure 12 and figure 13 are the 3 contours for the 4 sized glazed ice. It was already shown in section 4 that glaze ice generally had the worst lifting performance behavior and the most chaotic airflow conditions, and this group of x-velocity magnitude figures (figure 11) provided another supporting evidence. From 0.75x size 3 small vortices already emerged in the upper leading edge, bottom airfoil and the trailing edge of the airfoil. The generation of the trailing edge vortex in the 0.75x stage would actually be a surprise since 1x size did not show such a vortex. The potential cause for this vortex could be the special orientation of the upper size ice profile and leading edge vortex that disabled the flow to the trailing edge of the upper surface, supported by the decreased flow velocity in the corresponding locations shown on the contour. Despite these, it would be easy to anticipate the continuous growth of the upper and lower leading edge vortices as the icing profile increased that caused more air to be blocked. Until 1.5x ice size the vortices on both sizes were able to spread to the entire airfoil surface, disable the function of the entire airfoil, and totally mess up the airflow (even negative flow velocities) in the upper surface. This rapid increase of vortex would explain the dramatic decrease in lift coefficient observed previously.

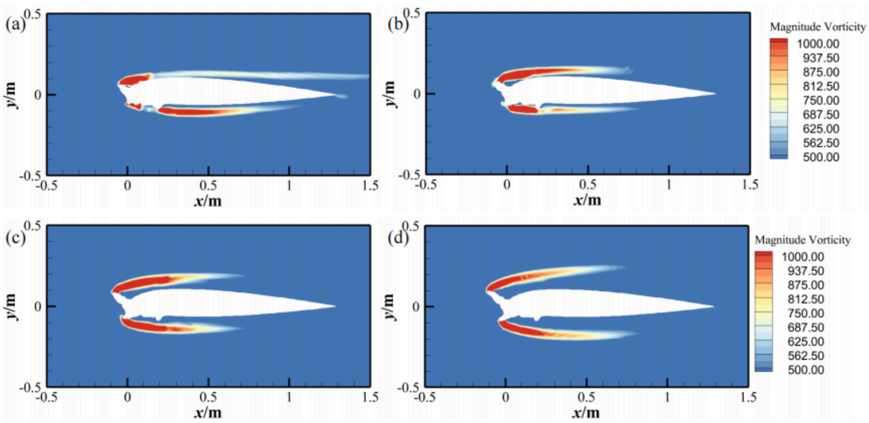

Figure 13. Contours of the pressure coefficient for: (a) 0.75x glaze ice, (b)1x glaze ice, (c) 1.25x glaze ice, and (d) 1.5x glaze ice

DOI: 10.54254/2753-8818/2026.HZ30765

The pressure coefficient contour showed an increased pressure in the leading edge as the icing profile increased, a typical phenomenon when there are icing conditions or other disturbances in the leading edge. The contour was also able to exhibit the special low pressure region behind the outstanding ice profiles, which partially explained the source of those large votives observed in the velocity magnitude contour. Finally, the vorticity contour suggested occurrence of vortices at the vertices of the icing profiles, and they were growing larger and larger as the icing profile size increased, aligning with the trends of both the previous 2 contours. In general, these 3 contours illustrated the numerical lifting results well, and multiple airflow characteristics were able to be found.

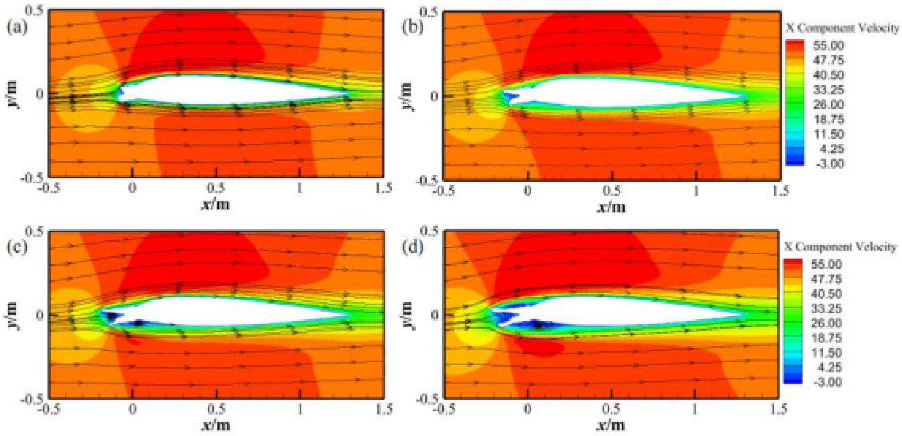

Figure 14. Contours of the $x-$ component velocity for: (a)0.75x horn ice, (b)1x horn ice, (c)1.25x horn ice, and (d)1.5x horn ice

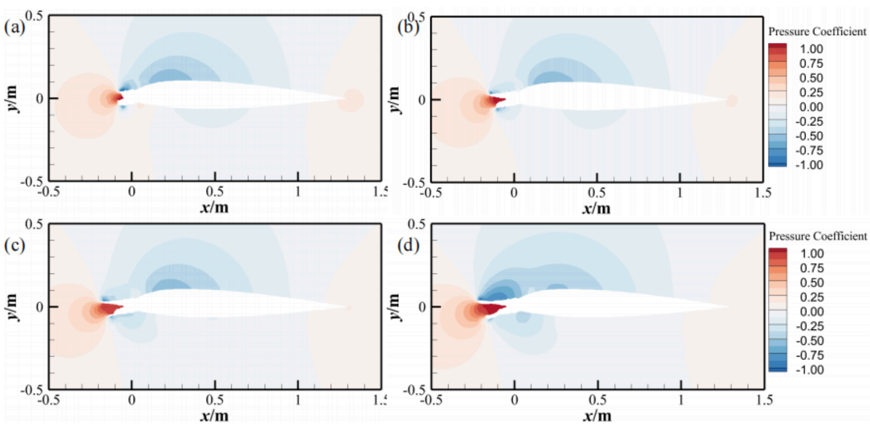

Figure 15. Contours of the pressure coefficient for: (a)0.75x horn ice, (b)1x horn ice, (c)1.25x horn ice, and (d)1.5x horn ice

Second, figure 14, 15 and 16 are the 3 contours for the horn ice profiles. Looking first again at the velocity magnitude, the 0.75x and 1x figures both showed really ideal airflow conditions, with the boundary layer lying tight to the airfoil and the streamlines showing no signs of vortices. Although due to the blocking of airflow from the horns the area of decreased airflow velocity seemed to be larger compared to the initial ideal smooth airfoil, the first two profiles still showed good airflow characteristics. However, vortices started to form in the 1.25x and 1.5x horn ice conditions. There are 2 vortices in total, one in between the 2 horns, which was a fairly reasonable

DOI: 10.54254/2753-8818/2026.HZ30765

place of occurrence as discussed earlier; The other one is in the bottom, which occurred due to the block of the airflow by the icing profile. Both these 2 vortices severely disrupted airflow and caused the performance reduction shown in the lifting data.

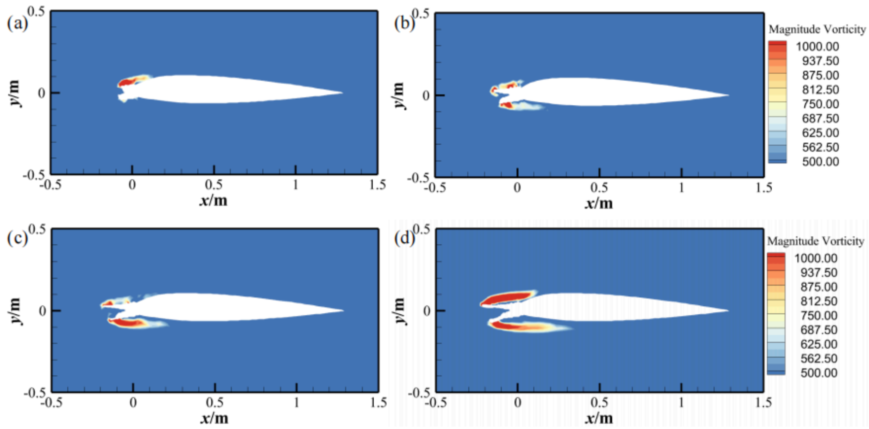

Figure 16. Contours of the pressure coefficient for: (a)0.75x horn ice, (b)1x horn ice, (c)1.25x horn ice, and (d)1.5x horn ice

The pressure coefficient assisted to validate this, as a relatively low pressure zone was found on the location of the vortices of the 1.25x and 1.5x icing profiles, serving as an indicator of the occurrence of vortex. This occurrence of low pressure at the bottom surface would directly lead to a copious amount of loss in lift produced, visualizing the dramatic decrease in lift coefficient. Additionally, the vorticity magnitude directly exhibited a growing trend of the vertex vortices as the icing profile increased, also aligning with the existing data. Comprehending all 3 figures, the reasoning for the exceptionally optimistic lift data performance of the 0.75x horn ice is likely due to the short length of the icing profile that enabled the airflow to perform normally.

Last, when visualizing the good but irregular performance of the rime ice profiles in figure 17, 18 and 19, what was seen was that the addition of the rime ice had almost no effect on the general pressure distribution, airflow direction and vortex generation of the airfoil. Only small abnormal pressure zones and vortices were evident in the icing profile, which was caused only by the rough surfaces of the ice. Those small ones did not show signs of spread as the icing profile size increased, which ensured the best lifting performance out of all 3 of the icing types. As long as the ice is smooth enough the rime ice configurations could even have a positive effect on the airfoil since it elongates the airfoil without changing the wanted dimensions and thus increases the lifting efficiency.

To summarize this section of analysis, the 4 icing profile sizing variance showed relatively different outcome: The glaze ice received a total destroy of lift as the ice size increased due to the large votives observed, originated from the lengthened ice vertex in both sides; The horn ice showed slightly more moderated performance while the generation of vortices and signs of flow separation in 1.0x and 1.25x icing sizes still worsened the lifting performance; The rime ice seemed to have the most optimistic performance, with changing the dimensions of the icing profile resulting in no evident correlations. The contour figures in all 3 of these cases were able to illustrate thorough reasonings and evidence to explain the situations occurring in the lifting data section.

DOI: 10.54254/2753-8818/2026.HZ30765

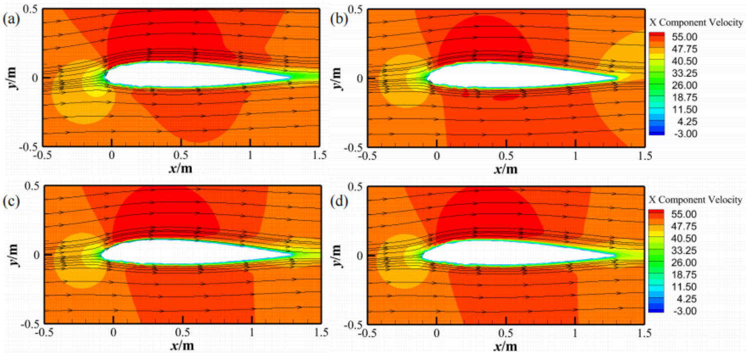

Figure 17. Contours of the $x-$ component velocity for: (a) 0.75x rime ice, (b)1x rime ice, (c)1.25x rime ice, and (d)1.5x rime ice

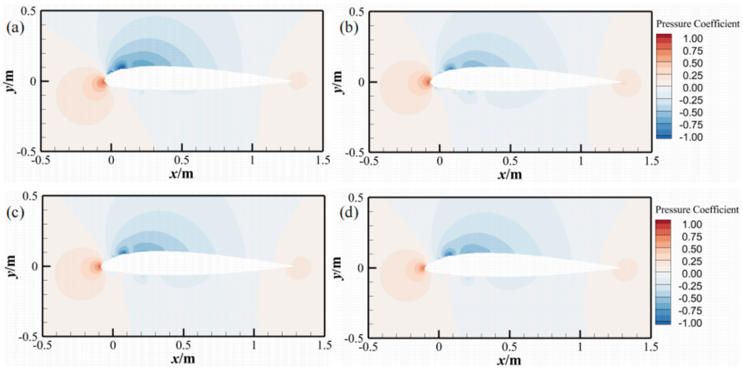

Figure 18. Contours of the pressure coefficient for: (a)0.75x rime ice, (b)1x rime ice, (c)1.25x rime ice, and (d)1.5x rime ice

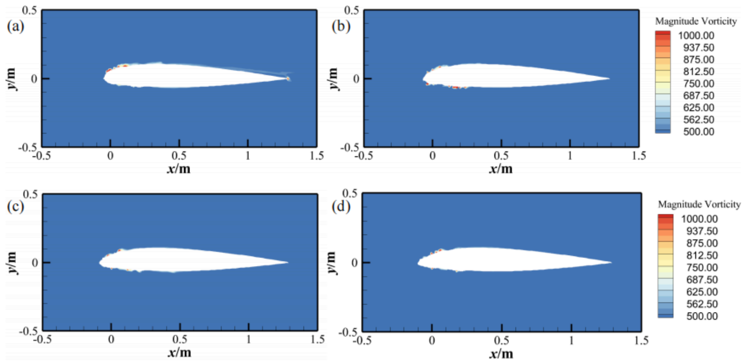

Figure 19. Contours of the pressure coefficient for: (a)0.75x rime ice, (b)1x rime ice, (c)1.25x rime ice, and (d)1.5x rime ice

5. Conclusion

This study investigated the aerodynamic characteristics of iced airfoils using CFD simulations. Key findings include:

1. Icing in general will decrease the lift performance of the airfoil by blocking the airflow and increase friction drag.

DOI: 10.54254/2753-8818/2026.HZ30765

2. Glaze ice produces the most severe aerodynamic penalties, reducing the L/D Ratio of the aircraft the most, mainly caused by the blockage of both sides of airflows to the airfoil that led to formation of large vortices.

3. Rime ice shows the least severe aerodynamic penalties, having the least amount of decrease in lift performance, caused by the tight attachment of its geometry to the airfoil that avoided the occurrence of vortices or unwanted air pressure changes.

4. Altering the icing sizes, length and thickness of the horn ice and glaze ice will have a large impact (negative relationship) to the performance of the airfoils, while will not have much variation and correlation to the rime ice.

5. Whether the icing profile blocks the airflow or constricts the airfoil function is the rudimentary logic and reasoning to the effect of icing on the airfoils.

6. Contour figures played a significant role in solidifying the reasonings for the occurrence of specific scenarios, assisting largely to the data analysis process.

Despite these basic findings, looking beyond the scope of this study only, the data provided by this research regarding the performance of airfoils under distinct icing conditions could serve as valuable resources for future researchers to consider during solidification of definitions of icing conditions, optimizations of airfoil dimensions, and finalization of aircraft safety documents. In general, the results of this research would be a good resource to support to overcome one of the largest threats to aviation safety – icing.

Lastly, discussing potential future works, future studies could first incorporate a systematic experimental data validation either by repeating the experiments with a different model or software, or use wind tunnels to verify the accuracy of the CFD. In this way the credibility of the data in this research could be elevated. Another possible future research would be to change the angle of attack, angle of sideslip, airspeed and a lot of other flight parameters during the simulation processes to acquire more comprehensive data. By doing so researchers will have a more full aspect of understanding regarding the exact outcome of icing conditions. Finally, it would also be possible to extend the current 2D airfoil into a full 3D aircraft configuration with the inclusion of fuselages, engines and other control surfaces, where in this way the realistic flight conditions could be modeled and the data acquired would be even more persuasive.

References

[1] Administration, F.A. (2024) In-flight Icing (IFI). https: //www.faa.gov/nextgen/programs/weather/awrp/ifi

[2] Board, N.T.S. Flying in Icing Conditions? https: //www.ntsb.gov/Advocacy/safety-alerts/Pages/SA-097.aspx

[3] Ranter, H. (2004) Accident Canadair CL-600-2B19 Regional Jet CRJ-200LR B-3072, Sunday 21 November 2004. Aviation Safety Network Database Entry. https: //asn.flightsafety.org/asndb/322511

[4] National Transportation Safety Board (1992) Aircraft Accident Report: Takeoff Stall in Icing Conditions, USAir Flight 405, LaGuardia Airport, Flushing, New York, March 22, 1992, Fokker F-28, N485US. Washington, D.C. https: //libraryonline.erau.edu/online-full-text/ntsb/aircraft-accident-reports/AAR93-02.pdf

[5] Ranter, H. (1992) Accident Fokker F-28 Fellowship 4000 N485US, Sunday 22 March 1992. Aviation Safety Network Database Entry. https: //asn.flightsafety.org/wikibase/325565

[6] FAA, Flight Safety Branch Aircraft Icing. Safe Pilots. Safe Skies. Safety Advisor; AOPA Air Safety Foundation. https: //www.aopa.org/-/media/Files/AOPA/Home/Pilot-Resources/ASI/Safety-Advisors/sa11.pdf

[7] National Weather Service Icing Hazards. Training Page, Weather.gov. https: //www.weather.gov/source/zhu/ZHU_Training_Page/icing_stuff/icing/icing.htm

[8] Cheung, M., Hann, R. and Johansen, T. (2022) UAV Icing: A Unified Icing Severity Index Derived from Performance Degradation. AIAA AVIATION 2022 Forum. https: //doi.org/10.2514/6.2022-3906

[9] Nath, P., et al. (2024) Parametric Investigation of Aerodynamic Performance Degradation Due to Icing on a Symmetrical Airfoil. Physics of Fluids, 36, 7.

DOI: 10.54254/2753-8818/2026.HZ30765

[10] Grainger Engineering Office of Marketing and Communications Computational Fluid Dynamics. Aerospace Engineering Research Area, University of Illinois Urbana-Champaign. https: //aerospace.illinois.edu/research/research-areas/computational-fluid-dynamics
[11] Addy, H.E.P. Jr., Broeren, A.P., Potapczuk, M.G., et al. (2016) Ice Accretions and Full-Scale Iced Aerodynamic Performance Data for a Two-Dimensional NACA 23012 Airfoil. NASA (via U.S. Army Aviation; Missile Research, Development; Engineering Center), Technical Report.
[12] Lednicer, D. (2025) The Incomplete Guide to Airfoil Usage. Website. https: //m-selig.ae.illinois.edu/ads/aircraft.html
[13] Leishman, J.G. (2023) Aerodynamics of Airfoil Sections. In: Introduction to Aerospace Flight Vehicles. Eagle Pubs. https: //eaglepubs.erau.edu/introductiontoaerospaceflightvehicles/chapter/airfoil-characteristics/